Biocomposite spheres based on aluminum oxide dispersed with orange-peel powder for adsorption of phenol from batch membrane fraction of olive mill wastewater

Jacques Romain Njimou [a,c,*], John Godwin [b,f], Hugues Pahimi [a], S. Andrada Maicaneanu [c,**], Fridolin Kouatchie-Njeutcha [d], Bankim C. Tripathy [b], André Talla [d], Toru Watanabe [e], Nkeng George Elambo [d]

[a] School of Chemical Engineering and Mineral Industries, University of Ngaoundere, P. O Box 454, Ngaoundere, Cameroon
[b] Hydro & Electrometallurgy Department, Institute of Minerals and Materials Technology, Bhubaneswar 751 013, India
[c] Madia Department of Chemistry, Indiana University of Pennsylvania, Indiana, PA 15705, USA
[d] Research Center, National Advanced School of Public Works, P.O. Box 510, Yaounde, Cameroon
[e] Deparment of Food, Life & Environmental Sciences, Faculty of Agriculture, Yamagata University, 1-23 Wakaba-machi, Tsuruoka, Yamagata 997-8555, Japan
[f] Department of Chemistry, Kogi State College of Education (Technical), P.O.B 242 Kabba, Nigeria

ARTICLE INFO

ABSTRACT

A novel multi-function material from secondary resources was synthesized using a facile protocol to convert available 'no value waste' into a friendly, cost-effective, and highly selective new filtering material suitable for usage in developing countries. This newly prepared material was used to separate valuable phenols like hydroxytyrosol from toxic phenol. Orange-peel aluminum biocomposite was synthesized via hydrothermal method, characterized, used to manufacture alginate spheres (Alg/OP-Al), and tested in batch and fixed-bed conditions. Batch results showed that phenol exhibited single (39.60 mg g^{-1}) < binary (92.75 mg g^{-1}) sequence, while hydroxytyrosol displayed single (41.50 mg g^{-1}) > binary (40.00 mg g^{-1}) sequence. The fixed-bed approach showed that during the intermediate stage, adsorbed hydroxytyrosol molecules were substituted by the influent phenol molecules, as a result, hydroxytyrosol outlet concentrations were higher than the inlet ones. Alg/OP-Al spheres allowed efficient separation of phenol and hydroxytyrosol with up to 90% purity from OMWW.

1. Introduction

Olive mill wastewater (OMWW) generated during olive oil production is harmful to organisms and human health due to its high phenol content [1]. Because of this, the generated streams are extremely dangerous for the environment, especially when do not undergo any treatment or applied directly on the ground without any control. This results in a negative impact on the environment which results in clogging of soil, pollution of surface and groundwater, and the release of noxious odors. OMWW is a typical agro-food wastewater i.e. phytotoxic, resistant to biological treatment, and harmful to flora and fauna [2–4]. The Environmental Protection Agency has set agro-food water purification standard to less than 1 ppb of phenol before discharge in surface

waters, while European Union standard recommends phenol allowable limit in drinking and mineral waters of 5 μg L^{-1}, 0.5 mg L^{-1} for wastewater emissions, and 1 mg L^{-1} for surface waters and sewage systems [5]. Laws have proved that good environmental practices could help to save money and create new business opportunities since the waste can be transformed into commodities. Recovering the polyphenol fraction of OMWW would facilitate the waste disposal and produce a natural extract characterized by high antioxidant power which may attract the attention of pharmaceutical, cosmetic, and food industry [1,2].

Several processes have been developed for the treatment of OMWW. These techniques include chemical precipitation, flocculation, ion exchange, electrolysis, membrane processes, and adsorption [2,4,6–8].

The sequential cross-flow processing of OMWW includes: sieving at 300 μm, pre-treatment processes by coagulation and flocculation, and membrane process composed of ultrafiltration, nanofiltration, and reverse osmosis. The fraction obtained at the end of the batch membrane operation appeared to be rich in polyphenols and should be processed for their recovery in regards to the negative impacts of phenols.

Given that existing technologies for phenol removal are technically complicated, expensive, and generally unsuitable for developing countries, this work proposes the development of a novel multi-function filter from secondary resources using a facile and versatile protocol to convert easily available 'no value waste materials' into valuable water filtration products. Agro-food based economies generate an abundance of wastes in the form of crop and plant residues. One of these residues, orange-peel (OP), is composed mainly of cellulose, pectin, hemicellulose, lignin, chlorophyll pigments, and low molecular hydrocarbons with many hydroxyl functional groups. Therefore this material will present adsorptive properties that can be successfully used for removal of many pollutants from waste water [9,10]. However, most of the wastes are still largely under-utilized and left to rot or openly burnt in the field. Most often, poor management of such wastes results in a number of environmental and health issues [11–13]. Therefore, orange-peel waste conversion into porous (nano) materials and the combination of oxide with polymers to produce new filtration systems for water treatment is novel and presents an exciting opportunity towards sustainable safe water production for all people while addressing waste recycling and circular economy. These newly developed (nano)materials can be useful through cost savings, resource recovery, and protection of the environment from wastes [14,15].

The use of orange-peel powder as robust support blending Al_2O_3 composite designed to remove phenol from sequential cross-flow membrane processing of OMWW was considered in this study. Low-cost materials were used to develop a new matrix for embedding active aluminum oxide nanomaterial able to separate phenol from compounds of interest in agro-food waters, a realistic alternative to the existing technologies. The adsorptive properties of hydrothermal biocomposite spheres based on aluminum oxide dispersed with orange-peel powder open new insights into the field and to the best of our knowledge there is no previous study devoted to a similar material used for the purpose of separation. Alginate aluminum-orange-peel (Alg/OP-Al) spheres were hydrothermally synthesized, chemically stable, and used in batch and in a fixed-bed column to remove phenol and hydroxytyrosol. Phenol and hydroxytyrosol in single and binary solutions were used as model adsorbates of phenolic compounds for elucidating the multi-component adsorption process frequently occurring in OMWW. The selective adsorption of phenol and hydroxytyrosol from aqueous solutions were experimentally investigated and the achieved optimal operating conditions were applied to nanofiltrate of OMWW.

2. Materials and methods

2.1. Materials

Orange-peel (OP) was collected from orange vendors in Yaounde, washed to eliminate dust on the surface, and dried at room temperature.

Aluminum sulfate hydrate (98%), sodium hydroxide ACS reagent ($\geq$ 97.0%), and sodium alginate (90.8–106.0%) were purchased from Sigma-Aldrich. Phenolic compounds tyrosol (99.5%), 3,4-dihydroxybenzoic acid (97%), vanillic acid (97%), and p-coumaric acid (98%) were obtained from Fluka. Hydroxytyrosol (98%), catechin hydrate (98%), caffeic acid (99%), rutin (94%), syringic acid (95%), and phenol (99%) were all acquired from Sigma Aldrich. All these standards were of HPLC grade. Analytical grade solvents acetonitrile (HPLC grade) by J.T Baker and ethanol 99.8% by Fluka were also used.

Phenol and hydroxytyrosol single and binary model solutions were prepared in bi-distilled water at a concentration of 600 mg L^{-1}. A binary solution contains equimolar amounts of phenol and hydroxytyrosol. The

value of the concentration was selected based on the results obtained in a previous study [16].

OMWW was collected from the PHOTOMEM pilot plant located at LABOR facilities in Via Giacomo Peroni 386, 00131 Rome and handled as previously described [17].

2.2. Hydrothermal synthesis of the biocomposite

Peels were washed with deionized water to remove physically adsorbed contaminants, dried at 40 °C for 72 h, grounded and sieved to obtain a powder with particles size between 0.1 and 0.2 mm thus to increase their surface area [9,10]. Thereafter, 15 g of powder was boiled in 250 mL deionized water at 80 °C for 1 h, vacuum filtered, and stored at 4 °C. Since OP also contain phenolic compounds, the powder was washed and extracted by ultrasound-assisted extraction according to Ververi and Goula [10] to remove all its phenolic content as well as all the extractible, therefore avoiding their release during the adsorption experiments. A blank test was run to follow the possible leaching behavior of the newly prepared composite.

Biocomposite material was hydrothermally synthesized using an adaptation of a procedure described by Tchomgui-Kamga et al. [18,19]. As shown in Fig. 1, the synthesis of the aluminum nanomaterial (OP-Al) was carried out by adding the orange-peel material previously obtained to a 0.10 M $Al_2(SO_4)_3$ solution with a volume ratio of 2:1 at room temperature, dispersed into a beaker containing 30 mL of 1 M NaOH and constantly stirred for 30 min. For the synthesis of OP-Al powder, a hydrothermal method was developed (Fig. 1A). The obtained paste was homogenized in an agate mortar and placed into a Teflon autoclave filled with 100 mL of distilled water. Then, the autoclave was sealed and placed in the oven at 110 °C for 12 h [12]. The prepared OP-Al biocomposite was separated by vacuum filtration and dried under vacuum. The obtained nanomaterial was washed with ethanol and distilled water, dried, and further used to prepare the alginate beads.

2.3. Preparation of biocomposite spheres

Alginate-aluminum orange-peel (Alg/OP-Al) spheres (Fig. 1B) were prepared by mixing 0.25–1.5 g of OP-Al powder with 1 g of sodium alginate dissolved in 1 mL of EtOH and an amount of water varying between 20 and 35 mL according to Njimou et al. [16]. The mixture was blended to obtain a homogenous mixture, then poured into a 0.2 M solution of CaCl$_2$ with the aid of a 1.2 mm diameter needle syringe, which resulted in the formation of beads with diameters between 1.5 and 2.0 mm. Once the biocomposite spheres (Alg/OP-Al) were formed, stirring was stopped and the beads were let to rest for at least two hours. Then they were removed, washed, conserved in demineralized water, and spin-dried before further use.

2.4. Characterization techniques

The morphology of OP-Al material was examined using a JOEL-IT 300 Scanning Electron Microscope (SEM) instrument coupled with energy-dispersive X-ray spectroscopy (EDS). Before analysis, samples were placed on double-sided carbon conductive tape and were double coated with carbon using a Quorum Q150R ES instrument. The phase structure was determined by X-ray analysis (XRD) using diffractograms recorded with a Bruker diffractometer system EMPYREAN with CuKα radiation. Each sample was scanned within the 10–90° 2θ range. The measurements were performed at a scan rate of 24.765 s and a step size of 0.0170°. Thermal gravimetric analysis (TGA) was conducted with a TG-DSC instrument (SETARAM KEP Technologies SETSYS Evolution) within 20 to 1000 °C temperature range using a 10 °C min^{-1} heating rate in N$_2$ atmosphere. Fourier Transformed Infrared (FTIR) spectra were recorded at room temperature within a spectral range of 500–4500 cm^{-1} using an Alpha-P Bruker spectrophotometer. OP and OP-Al samples were prepared by encapsulating 1.2 mg of finely grounded dried powder
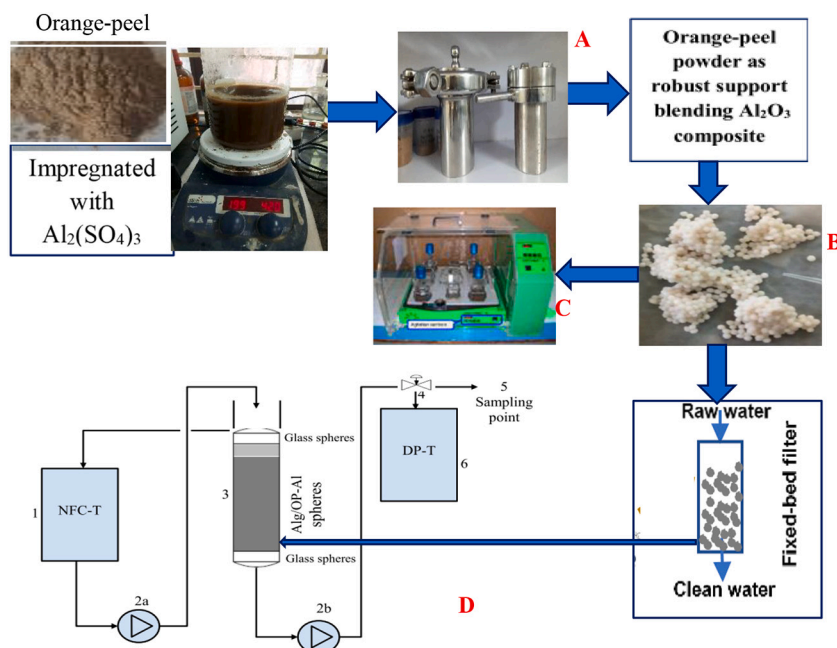
Fig. 1. Schematic diagram of hydrothermal synthesis (A), biocomposite spheres (B), batch orbital incubator(C) and fixed-bed (D) experimental setups 1) NFC-T: Nanofiltration concentrate tank; 2a, 2b- Displacement pump; 3) Column; 4) Three-way valve; 5) Sampling point; 6) DP-T: De-phenolized water tank.

particles in 300 mg of KBr.

2.5. Adsorption and desorption experiments

Batch experiments were conducted at 25 °C using 10 g of spin-dried biocomposite spheres (corresponding to a dry weight of 1.5 g). The spheres were added to several 200 mL aqueous solution samples of known phenol and hydroxytyrosol concentration (50 to 500 mg L^{-1}) in a 500 mL sealed flask. Afterwards, the flask was shaken at 150 rpm at constant temperature in a Certomat Orbital incubator shaker (Fig. 1C), equipped with a thermostat, for 3 h until equilibrium was reached. Samples were collected at specified time intervals. All experiments were conducted at the same pH, that of the initial solution (pH 5.4). The equilibrium concentration of phenol and hydroxytyrosol on the solid phase, q$_e$ (mg g^{-1}), was calculated as follows:

$$q_e = (C_0 - C_e)\frac{V}{m} \tag{1}$$

Where C$_0$ and Ce (mg L^{-1}) are the initial and the equilibrium phenol and hydroxytyrosol concentrations in the liquid respectively, V (L) is the initial volume of liquid, and m (g) is the initial mass of the spheres. The optimum parameters (mass, pH, equilibrium time) were obtained experimentally.

Continuous fixed-bed adsorption runs were performed in a glass column (4.0 cm in diameter and 40 cm in length), in downflow mode. The Alg/OP-Al composite beads, 680 g L^{-1} (4.0 cm bed height, Z) were packed in the column with two layers of glass spheres at the top and bottom, respectively, as shown in Fig. 1D. The phenol and hydroxytyrosol in single or binary (equimolar) solutions at an initial concentration of 600 mg L^{-1} were fed in the column using a peristaltic pump. A second peristaltic pump at the exit of the column was used to ensure that the flow rate was maintained constant throughout the experiments (0.8, 1.3, 2.0, and 4 mL min^{-1}). Effluent samples were collected at specified intervals (up to 35 h) and analyzed for the residual phenolic concentration using an Agilent Technologies 1200 HPLC system fitted with a SUPEL-COSIL LC-18 column (4.6 mm × 250 mm, 5 μm i.d., Teknokroma) at a fixed temperature of 20 °C. The separation was achieved in gradient mode using acetic acid in bi-distilled water 0.5% (A) and acetonitrile (B). The eluent composition initially equal to 100% (A), was changed

gradually to 55% (A) and 45% (B) in 45 min, then again gradually to the initial solvent composition to the end of the run. The analysis time was set at 60 min, the effluent flow rate was 1.0 mL min^{-1}, and the detection wavelength was set at 280 nm. The composition of phenolic compounds in the samples was based on the peak area of standards. This technique allowed excellent concentration measurements since the linear correlation coefficients (R^2) between predicted and real values were higher than 0.99 [17].

The loading behavior of Alg/OP-Al composite in fixed bed to remove phenol and hydroxytyrosol was expressed in normalized concentration defined as the ratio of effluent solute concentration to inlet (feed) solute concentration (C/C$_0$), as a function of time or volume of effluent for a given bed height. The adsorption performance for a given-bed mass was directly related to the number of bed volumes (BV) processed before the breakthrough point is reached. Effluent volume (V) was determined using Eq. (2):

$$V = Q \cdot t \tag{2}$$

where Q is the volumetric flow rate (mL min^{-1}) and t is the total flow time (min).

To select phenol from hydroxytyrosol in a binary system or nanofiltration concentrate of OMWW, the hydroxytyrosol solution with 100% purity was represented by a time (min) in which the effluent contains only hydroxytyrosol since its breakpoint (B.T$_{Ho-Ty}$ = Breakthrough time):

$$\Delta V_{100} (mL) = Q(time_{(100\%)} - time_{(B.T)}) \tag{3}$$

In binary components, the hydroxytyrosol separated with 90% represents a time (min) in which the outlet contains hydroxytyrosol at 90% and phenol at 10% since its breakpoint (B.T) as:

$$\Delta V_{90} (mL) = Q(time_{(90\%)} - time_{(B.T)}) \tag{4}$$

As well, in a multi-component system of nanofiltration concentrate of olive wastewater, a phenolic solution with 100% purity represents a time (min) in which the outlet stream contains the target polyphenols in the study which are hydroxytyrosol and rutin at 100% purity towards phenol since their breakpoint (B.T) as:

$$\Delta V_{100}*(mL) = Q\big(time_{(100\%)} - time_{(B.T)}\big) \tag{5}$$

Hydroxytyrosol-rutin with 90% purity represents a time (min) in which the effluent contains only hydroxytyrosol and rutin at 90% and phenol at 10% since its breakpoint (B.T) as:

$$\Delta V_{90}*(mL) = Q\big(time_{(90\%)} - time_{(B.T)}\big) \tag{6}$$

3. Results and discussion

3.1. Materials characterization

3.1.1. Structural characterization

SEM image of composite material (OP-Al) is presented in Fig. 2A. OP-Al adsorbent presents a fibrous structure and a stick surface morphology.

The EDS analysis of OP-Al (Fig. 2B) showed that they mainly contain C, while certain amounts of Al and Si were also detected. Based on these facts, it can be concluded that the synthesized OP-Al material presented an adequate morphology for the accumulation of pollutants.

The XRD patterns for the OP and OP-Al, recorded with PAN analytical X'Pert High Score software, are presented in Fig. 2C. The calculated lattice parameters for OP-Al nanomaterial were as follows 3.50258 Å, 3.34643 Å, and 2.21137 Å and correspond to α- Al_2O_3, quartz, and stishovite, respectively which indicated that Al_2O_3 was successfully incorporated in the orange-peel powder blended composite. The lattice parameter of 3.34242 Å for OP corresponds to Graphite 2H [12,18,19].

In order to study the thermal stability of OP-Al, a differential thermal gravimetric (DTG) curve was recorded at 10 °C min^{-1} (Fig. 2D). The peak centered at 303.29 °C is correlated to an endothermic effect (93.73 J g^{-1}) due to the evaporation of physically adsorbed water and the decomposition of epoxy and carboxyl groups. The peak observed at about 715.58 °C is correlated to an endothermic effect (171.307 J g^{-1}) linked to exfoliation in the OP-Al nanomaterial during treatment at high
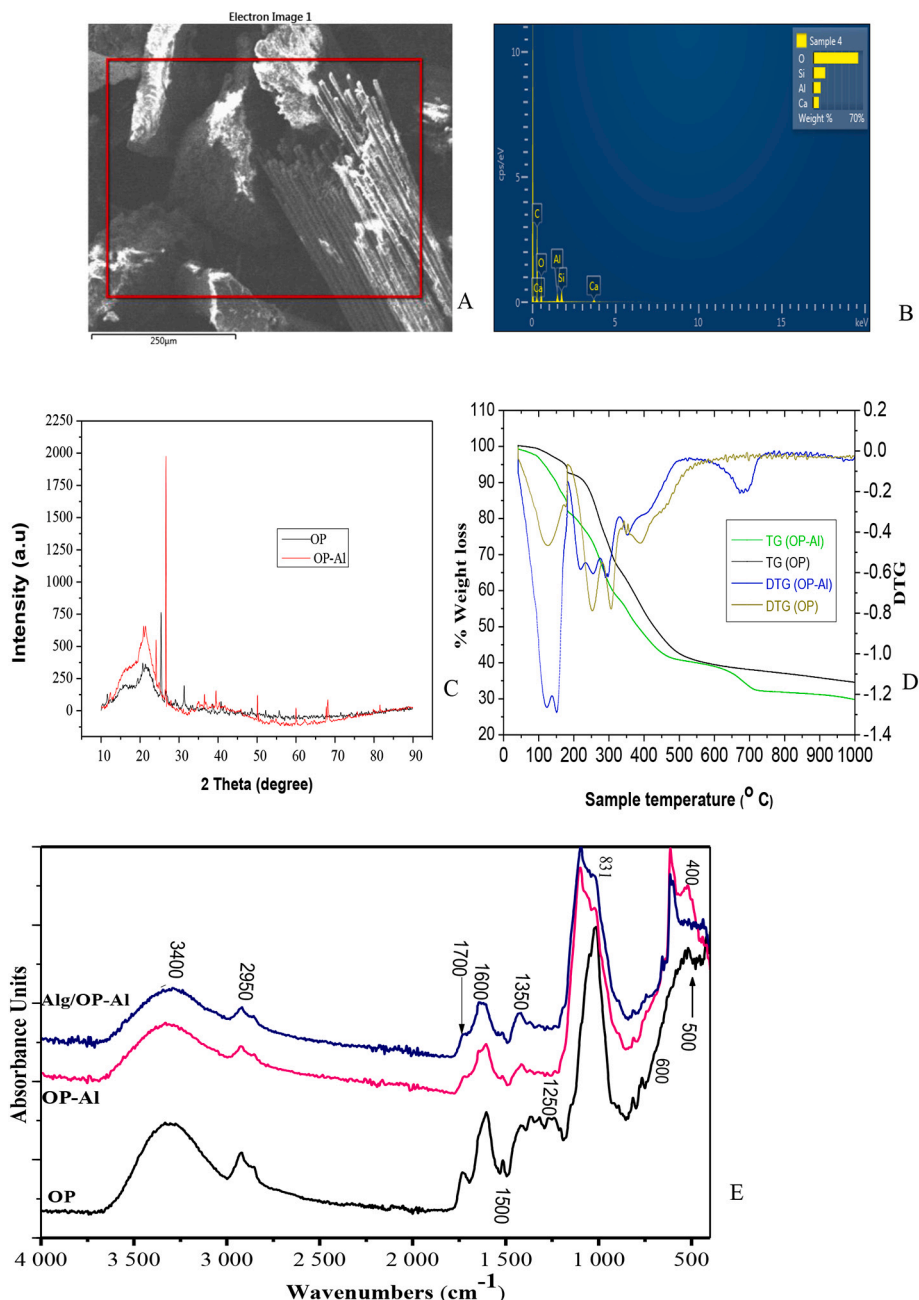

Fig. 2. SEM (A), EDX (B), XRD (C), TG and DTG (D), and FTIR spectra (E) of OP, OP-Al, and Alg/OP-Al.

temperature. The total weight loss of 69.8% was observed at 983.81 °C, corresding to a loss of mass from 27.0 mg to 17.5 mg. The weight loss is related to the gradual dehydration/dehydroxylation of aluminum oxides [20,21].

The isoelectric potential of the material in a solution is the pH value at which the net surface charge of the material is equal to zero. At this value, the adsorbent is neutral, while it turns positively charged at lower pH values or negatively charged at higher pH values [22]. The bio-composite based on aluminum oxide dispersed with orange-peel powder (OP-Al) is a porous nanomaterial. The point of zero charge of bio-composite was 6.2 explaining by the fact that for initial pH values below 6.2 [9], the protons in solution migrate into composite spheres and protonated material above 6.2, protons are released from biocomposite into the solution, resulting in bearing an overall negative charge.

3.1.2. Spectroscopic analysis

The FTIR analysis of the OP, OP-Al, and Alg/OP-Al samples was employed to study the change in chemical functional groups. The obtained spectra are presented in Fig. 2E. The broad and intense absorption peaks at 3400 cm^{-1} correspond to the O—H stretching vibrations of cellulose, pectin, hemicellulose, and lignin. The peaks at 2950 cm^{-1} are attributed to the C—H stretching vibrations of methyl, methylene, and methoxy groups. The peak observed around 1750 cm^{-1} is the stretching vibration of the C—O bond due to non-ionic carboxyl groups (-COOH, -COOCH$_3$), and might be assigned to carboxylic acids or their esters. The peaks at 1638 cm^{-1} are due to the C=C stretching that can be attributed to the presence of aromatic or benzene rings in lignin. The peaks at 1000 cm^{-1} were assigned to the C—O stretching vibration of carboxylic acids and alcohols [16,17]. Meanwhile, it can be observed that the obtained OP-Al and Alg/OP-Al showed new peaks around 520 cm^{-1} that were attributed to the O-Na-Al and O—Al bonds [13]. The peak is more intense for OP-Al than Alg/OP-Al which confirmed the successful preparation of support blending Al$_2$O$_3$ composite and proved that Al is effectively grafted into the composite materials.

3.2. Application of orange peel biocomposite spheres

3.2.1. Batch adsorption

The adsorption of phenol and hydroxytyrosol onto Alg/OP-Al spheres was carried out in single and equimolar-binary components and the collected data were fitted to Langmuir and Freundlich isotherm models, Fig. 3. Langmuir isotherm states that the adsorbed molecules occupy the finite adsorption sites of homogenous surface by monolayer adsorption and there is no interaction between adsorbed molecules
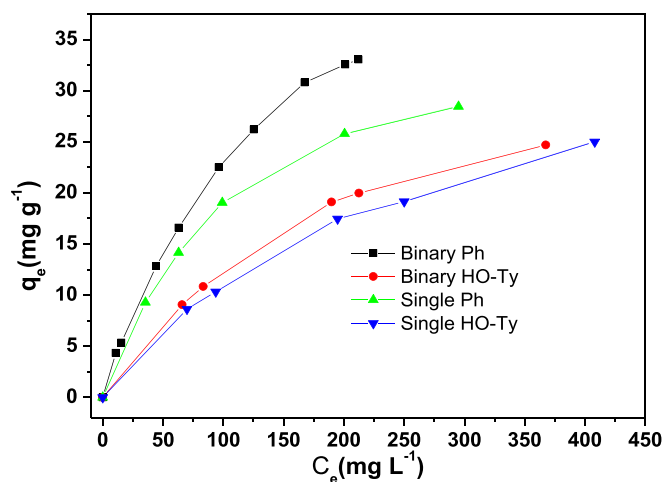
during the adsorption process. The linear form of Langmuir isotherm is expressed by Eq. (7) [16,23]:

$$\frac{C_e}{q_e} = \frac{C_e}{q_{max}} + \frac{1}{q_{max}K_L} \tag{7}$$

where q_e and q_{max} (in mg g^{-1}) represent the adsorption capacities of solute at equilibrium and the maximum amount adsorbed respectively, K_L (L mg^{-1}) is the Langmuir equilibrium constant related to the affinity of binding sites and energy of adsorption, and C_e (mg L^{-1}) is the equilibrium concentration of substrates in solution. Values of K_L and q_{max} were calculated from the intercept and slope of the liner plot of experimental data of C_e/q_e versus C_e. A dimensionless constant of the Langmuir equation called the equilibrium parameter R_L was defined as follows [16,17,24,25]:

$$R_L = \frac{1}{1 + C_0 K_L} \tag{8}$$

where C_0 (mg L^{-1}) is the highest initial concentration. R_L value indicates the type of isotherm to be irreversible adsorption ($R_L = 0$), favorable adsorption ($0 < R_L < 1$), unfavorable adsorption ($R_L > 1$), and linear adsorption ($R_L = 1$). The closer to zero, the more favorable the adsorption.

Freundlich isotherm is based on the assumptions that the adsorption surface is energetically heterogeneous with an unlimited number of sites and the adsorbed molecules can interact with each other. The linear form of this model is expressed as follows [16,23,26]:

$$\ln q_e = \ln K_F + \frac{1}{n_F}\ln C_e \tag{9}$$

where K_F (in mg$^{1-1/n}$ L$^{1/n}$ g^{-1}) and n_F are the Freundlich parameters referring to the equilibrium constant and the adsorption intensity respectively and can be determined from the linear plot of $\ln(q_e)$ versus $\ln(C_e)$.

The factors affecting the efficiencies of phenol and hydroxytyrosol adsorption on the composite material were studied and the results showed that the adsorption reached equilibrium after 45 min. As shown in Fig. 3 the adsorption capacity increased with solute concentrations for all systems under the studied conditions. Phenol exhibited single < binary sequence, while hydroxytyrosol displayed single > binary sequence. The increase is the result of the accumulation of phenol in binary system onto biocomposite along to the driving force due to the phenol concentration gradient (from the solution to the adsorbent) as when the initial concentration increases.

As shown in Table 1, the data collected for single and binary systems fitted well on both Langmuir and Freundlich isotherm models ($R^2 > 0.960$). The values of R_L at $C_0 = 500$ mg L^{-1} were calculated to be less than 1 for both solutes indicating a favorable adsorption processes [23–25].

The calculated K_F and n values calculated for both solutes are given in Table 1. The n values for both single and binary systems were always

Fig. 3. Adsorption isotherms data for phenol and hydroxytyrosol adsorption onto Alg/OP-Al in single and binary systems at different solutions.

Table 1
Langmuir and Freundlich isotherms parameters determined using non-linear regression for phenol and hydroxytyrosol adsorption onto Alg/OP-Al composite.

Parameter	Single system		Binary system	
	Hydroxytyrosol	Phenol	Hydroxytyrosol	Phenol
Langmuir isotherm				
q_m (mg g^{-1})	41.50	39.60	40.00	92.75
q_{exp} (mg g^{-1})	30.30	28.42	31.50	69.40
k_L (Lm g^{-1}) 10^{-3}	3.63	9.00	4.60	3.01
R_L	0.40	0.20	0.30	0.40
R^2	0.993	0.998	0.994	0.999
Freundlich isotherm				
k_F	0.61	0.80	0.89	0.92
n	1.65	2.22	1.76	1.50
R^2	0.984	0.961	0.981	0.998

between 0 and 10, indicating the favorable adsorption of phenol and hydroxytyrosol onto Alg/OP-Al composite under the studied conditions [30].

The comparative values of adsorption capacities for phenol using various adsorbents by comparison with the Alg/OP-Al composite are shown in Table S01 (Supplementary material). It may be concluded that Alg/OP-Al spheres have certain advantages for phenol adsorption.

3.2.2. Column adsorption

3.2.2.1. Single and binary components. The results obtained for the adsorption of phenol and hydroxytyrosol in single and binary systems on Alg/OP-Al composite at ambient temperature are shown in Fig. 4. As the adsorbates concentration front moves throughout the bed, the breakthrough time (BT) where complete adsorption is not guaranteed anymore, will be reached first, followed by the plateau point time (PT), where complete exhaustion of the Alg/OP-Al beads composite is reached and therefore the concentration at the inlet is equal to that measured at the outlet. The influent flow rate, initial concentration, bed height, diameter of column, and Alg/OP-Al particle size were $Q = 2$ mL min^{-1}; $C_0 = 600$ mg L^{-1}, $Z = 4.0$ cm, $D = 4.0$ cm), respectively. Specifically, the volumes of water treated before breakthrough point ($C/C_0 = 0.01$; 13.25 h) and ($C/C_0 = 0.01$; 19 h) were 1440 mL and 2280 mL for hydroxytyrosol and phenol, respectively for single solutions. The time for reaching breakthrough point ($C/C_0 = 0.04$) was found to be 15.5 and 21 h for hydroxytyrosol and phenol, respectively in binary system (Fig. 4B).

Looking at both solutes, it is clear that in single and binary systems, the breakthrough curve has the same behavior for phenol as well as it appears later than that of hydroxytyrosol. This confirms that phenol is the strongly adsorbed compound due to its high affinity and selectivity for the adsorbent. For the hydroxytyrosol, the breakthrough course is steeper, and the breakpoint appears earlier. Therefore, the hydroxytyrosol solute is considered the weakly adsorbed component. These results are in agreement with those obtained by other researchers [27,28].

During the early stage of the column operation, the Alg/OP-Al composite bed possessed abundant adsorption sites for the incoming phenol and hydroxytyrosol. Almost all the phenol and hydroxytyrosol molecules were captured by the Alg/OP-Al bed. Therefore, the effluent phenol and hydroxytyrosol concentrations were very low. During the intermediate stage of the column operation, the adsorbed hydroxytyrosol molecules were replaced by the incoming phenol molecules due to the weaker affinity of hydroxytyrosol towards the Alg/OP-Al composite. This resulted in an intermediate zone with the effluent hydroxytyrosol

concentration higher than its feed concentration. The existence of such a high-concentration intermediate zone was also found by authors [28–32]. During the final stage, almost all the adsorption sites were occupied with the incoming phenol and hydroxytyrosol molecules, while Alg/OP-Al composite bed lost its adsorption capacity.

3.2.2.2. Effect of flow rate and the corresponding hydraulic retention time. The effect of flow rate in binary solutions (0.8, 2.0, and 4.0 mL min^{-1}) at influent concentrations of 600 mg L^{-1} are presented in Fig. S01 (Supplementary material) for hydroxytyrosol and phenol, respectively. Table 2 displays operating variables in respect to the effect of flow rate and the corresponding hydraulic retention time (HRT). HRT is defined as the ration between the bed volume and the flow rate. When the flow rate increases (0.8 to 4.0 mL min^{-1}), Table 2, the HRT decreases sharply from 37.0 to 8.5 h and 32.0 to 6.5 h for phenol and hydroxytyrosol, respectively, confirming the residence time of each pollutant in the column. As a result, the adsorption equilibrium will no longer be reached at a higher flow rate, as phenol and hydroxytyrosol leave the column earlier, due to

Table 2
Effect of flow rate and selectivity in column approach by Alg/OP-Al beads.

Feed stream		Hydroxytyrosol and Phenol at 600 mg L^{-1}			
Feed flow rate (mL min^{-1})		0.8	1.3	2.0	4.0
Water resource at Hydroxytyrosol Breakthrough (BT$_{HO-Ty}$)	HRT (h)	32.0	21.5	11.5	6.5
	volume (mL)	1536	1677	1380	1560
Hydroxytyrosol solution at 100% at Phenol Breakthrough (BT$_{Ph}$)	HRT (h)	37.0	26.5	18.5	8.5
	volume (mL)	1776	2067	2220	2040
	ΔV_{100} (mL)	240	390	840	480
	m (mg)	19	31	66	14
	C$_{100}$ (mg L^{-1})	79.17	79.5	78.60	29.17
Hydroxytyrosol at 90% since BT$_{HO-Ty}$	HRT (h)	38.5	30.5	20.5	11.0
	volume (mL)	1848	2379	2460	2640
	ΔV_{90} (mL)	312	702	1080	1080
	m (mg)	65	222	325	201
	C$_{90}$ (mg L^{-1})	208.33	316.24	300.92	186.11
Phenol Plateau Time (PT$_{Ph}$)	time (h)	50	50	33	17
	volume (mL)	2400	3900	3960	4080
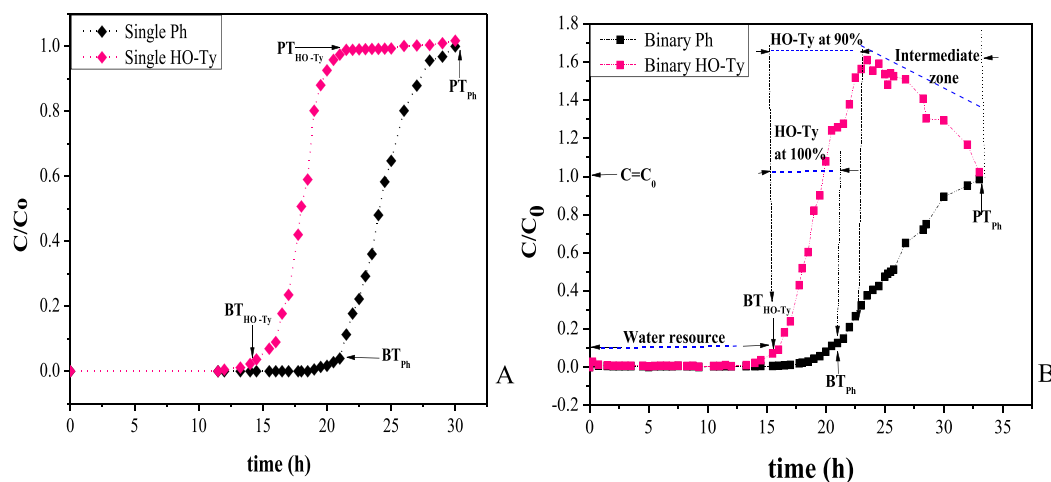
Fig. 4. Breakthrough curves in single (A) and binary (B) phenol (pH) and hydroxytyrosol (HO-Ty) onto Alg/OP-Al ($Q = 2$ mL min^{-1}, $C_0 = 600$ mg L^{-1}, $Z = 4.0$ cm, $D = 4.0$ cm).

the decrease in contact time. Higher uptake of phenol, as well as a faster selectivity for phenol, was observed compared to hydroxytyrosol. The adsorption of aromatic compounds onto Alg/OP-Al spheres is due to a combination of Van der Waals forces and thermodynamic gradient determined by the hydrophobicity which drives the molecules out of the aqueous solution. This is in agreement with the results obtained by other authors [33–35]. Based on literature data [34,36] the higher uptake of phenol in the binary system could be explained by the hydrophobic difference related to water solubility of the solutes, which at 298 K are 88.84 g L^{-1} and 67 g L^{-1} for the hydroxytyrosol and phenol, respectively. Furthermore, the greater electron density in which a ring of phenol molecules supplies more π-electrons to interact with the adsorbent results in a higher adsorption capacity [37,38].

Based on the results presented in Table 2, the fixed bed column approach is highly desirable for hydroxytyrosol and phenol removal from wastewater with hydroxytyrosol recovery as the concentration in the 'first bed' of effluent was almost zero for both solutes. The recovered water before the hydroxytyrosol HRT_{HO-Ty} was 1536, 1677, 1380, and 1560 mL at a feed flow rate of 0.8, 1.3, 2.0, and 4.0 mL min^{-1}, respectively. This effluent can be discharged directly or recycled to be processed as an additional water resource. From BT_{HO-Ty} to phenol breakthrough (BT_{Ph}) and the effluent up to 10% in phenol, the effluent containing mainly hydroxytyrosol with 100 and 90% in purity, respectively can be sent to a unit for hydroxytyrosol recovery.

The hydroxytyrosol solution at BT_{Ph} and effluent up to 10% in phenol were 240, 390, 840, and 480 mL; 312, 702, 1080, and 1080 mL at a feed flow rate of 0.8, 1.3, 2.0, and 4.0 mL min^{-1}, respectively with 100 and 90% in purity. For the effluent with more than 90% hydroxytyrosol BV, the Alg/OP-Al bed is saturated with the feed and regenerated to restore its adsorptive capacity.

3.3. Application of Alg/OP-Al spheres in a real scenario of nanofiltration concentrate

3.3.1. Nanofiltration feed stream

The wastewater that constitutes the feed stream (OMWW) used in this work it is the nanofiltration concentrate obtained after the raw olive oil wastewaters are subjected to a series of pre-treatments and membrane filtration processes. Previous studies showed that about 50% of the initial polyphenol content is destroyed through the flocculation and photocatalysis processes, while during the ultrafiltration process most of the polyphenols pass through the membrane [4,17,47]. As the ultrafiltration concentrate still contains some suspended solids, it is further subjected to nanofiltration. The choice of using the nanofiltration concentrate is not too convenient compared to the use of oil wastewater as there is a decrease in the concentration of polyphenols, but in reality, this decision is made especially for process reasons as the ultrafiltration concentrate is not recommended due to the presence of suspended solids which represent a potential fouling of the adsorption column.

Overall, the nanofiltration concentrate is the best choice among the possible feeds to be treated to recover polyphenols through an adsorption process in fixed-bed column and therefore to transformewastes into resources.

Referring to the retention times and areas (mAU) of the standards, it is possible to determine the mg L^{-1} of each individual polyphenol present in a sample of nanofiltration concentrate. Overall, it has been calculated that the concentrate of nanofiltration of olive vegetation waters is characterized by a total polyphenol concentration equal to 1691.496 mg L^{-1}. Concentration of identified polyphenols (mg L^{-1}) in the nanofiltration concentrate determined for the water used in this study are as follows: hydroxytyrosol (430), tyrosol (172), vanillic acid (70), caffeic acid (10.8), syringic acid (15) phenol (123.5), p-coumaric acid (14.8), rutin (124.01) [4,8,17,48].

3.3.2. Removal of phenol from nanofiltration concentrate

Alg/OP-Al spheres in fixed-bed were used in order to determine the adsorption effectiveness in this complex and realistic scenario i.e. OMWW. The influent flow rate was kept at a constant flow rate of 2 mL min^{-1} whereas the bed density, the bed height and the diameter of the column were ρ = 680 g L^{-1}, Z = 4.0 cm, D = 4.0 cm, respectively. Table 3 showed the resulting profiles while gathering the estimated breakthrough time with the following trend: Hydroxytyrosol < Rutin < Phenol.

As it can be seen in Table 3, a considerable reduction in breakthrough time was observed for hydroxytyrosol with the values of 12.0, 11.5, and 6.52 h in single, binary, and multiple component systems, respectively. Meanwhile, for phenol, the increase of breakthrough time was observed with 17.0, 18.0, and 22.65 h for single, binary, and multiple component systems. This results allowed a direct comparison with the data gathered in single and binary component solutions since the concentration swings were very similar. A quick comparison between the breakthroughs revealed that competitive adsorption is quite remarkable in the Alg/OP-Al bed composite studied. This showed that selectivity for phenol at BT increased in the order: single < binary < multiple (OMWW) onto Alg/OP-Al composite, while the contrary was observed for hydroxytyrosol at BT. The results are in agreement with those obtained in batch mode. This tendency is attributed to the competition between adsorbates for the same sites. Such adsorbates include hydroxybenzoic acids and its derivatives (gentisic, vanillic, gallic, syringic acids), cinnamic acids and derivatives such as caffeic, ferulic, sinapic acids, and phenolic alcohols, oleuropein, ligstroside, flavonols, flavones that frequently coexist in nanofiltration concentrate of agro-food water i.e. OMWW [5,6,39].

3.3.3. Desorption of phenol from Alg/OP-Al used spheres

After saturation, the Alg/OP-Al bed loaded by polyphenols was rinsed with deionized water. A 50% ethanol solution (v/v) was subsequently used as the desorption solvent for phenol from the Alg/OP-Al spheres. Desorption was carried out in the same conditions as adsorption i.e. the influent flow rate was kept at a constant flow rate of 2 mL min^{-1}, the bed height, and the diameter were Z = 4.0 cm, and D = 4.0 cm, at ambient temperature. 200 mL of 50% ethanol solution was passed through the Alg/OP-Al column and the concentrations of polyphenols were determined until the detection limit was reached. Once regenerated the fixed bed was subjected to the following adsorption-desorption cycle. Fig. 5 displays the results obtained during for the adsorption-desorption cycle using OMWW as feed and the mass balance for phenol, hydroxytyrosol, and rutin. The percent hydroxytyrosol, rutin and phenol desorbed were evaluated according to the formula [44,47,50]:

$$\text{Recovery efficiency } (\%) = \frac{q_{reg}}{q_{org}} \times 100 \tag{10}$$

$$q_{reg} = C_{reg} \times \frac{V}{W} \tag{11}$$

Table 3
Experimental results by using a nanofiltration concentrate of OMWW.

| Nanofiltration concentrate stream		Hydroxytyrosol	Rutin	Phenol
C (mg L^{-1})		172.12	124.01	123.55
Volume of treated water at Hydroxytyrosol Breakthrough (BT_{HO-Ty}) (mL)		782.4	782.4	782.4
$BT_{(component)}$	**time (h)**	6.52	8.35	22.65
	volume (mL)	780	1020	2700
Hydroxytyrosol and Rutin solution at 100% from BT_{HO-ty} (6.5 h) < BT_{Ph} (22.5 h)	**mass (mg)**	175.29	88.02	0.00
	C_{100} (mg L^{-1})	90.81	52.00	0.00
Hydroxytyrosol + Rutin at 90% from BT_{HO-ty}(6.5 h) to Phenol$_{(time at 10\%)}$	**time (h)**	28.0	28.0	28.0
	mass (mg)	229.4	138.05	9.30
	C_{90} (mg L^{-1})	88.92	53.22	3.41
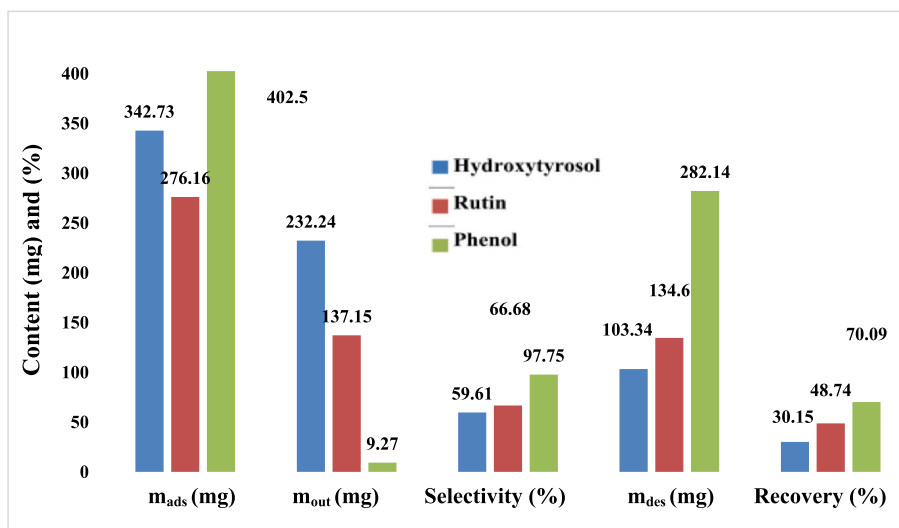
Fig. 5. Mass balance obtained from column adsorption data for OMWW (third regeneration cycle).

where, q_{reg} and q_{org} (mg g^{-1}) are the adsorption capacity of the regenerated column and the original adsorption capacity of the Alg/OP-Al spheres, C_{reg} (mg g^{-1}) is the concentration of phenolic in the solution with the volume V(L) and W (g) is Alg/OP-Al weight (g). As the adsorption/desorption cycles continued, the adsorption and desorption efficiencies gradually decreased. The results showed that the recovery efficiency was 30.15%, 48.74%, and 70.09% for hydroxytyrosol, rutin, and phenol, respectively after the third cycle by comparison with 32.02%, 49.84%, and 73.01% for the first cycle and the considered compounds. This might be explained by the deactivation of binding sites after repeated reuse and disintegration of beads during adsorption-desorption cycles. It appeared that phenol is adsorbed in a higher amount on Alg/OP-Al composite when nanofiltrate as a complex system was used compared to single and binary systems. The selectivity exhibited the following sequence sequence: hydroxytyrosol (59.61%) < rutin (66.68%) < phenol (97.75%). This selectivity sequence obtained for could be explained based on the hydrophobicity induced by the preponderance of phenolic compounds in multiple component systems [40–43,45,46,49]. Desorption of phenol as well for hydroxytyrosol and rutin from the saturated spheres proved to be faster than the adsorption by using 50% ethanol solution.

4. Conclusions

In summary, novel chemically stable alginate biocomposite spheres (Alg/OP-Al) were successfully manufactured and characterized. The experimental results show that the adsorption equilibrium of phenol and hydroxytyrosol was described by Freundlich and Langmuir models in batch mode. In single system column mode, the breakthrough region appears flatter for phenol and appears latter, confirming that phenol was the one stronger adsorbed onto the biocomposite spheres. Same observation was made for binary and nanofiltration concentrate of OMWW, hydroxytyrosol and rutin were the weakest adsorbed components, while phenol was the strongest adsorbed component. During the intermediate zone of adsorption, polyphenols initially adsorbed were replaced by the incoming phenol molecules displaying effluent concentrations higher than their feed concentrations. These results showed that the trend for phenol in BT is single < binary < multiple (OMWW), while the opposite was observed for hydroxytyrosol and rutin. Ethanol 50% (*v/v*) allowed the recovery of the considered polyphenols with selectivities of 30.15, 48.74, and 70.09% for adsorbed hydroxytyrosol, rutin, and phenol, respectively. The newly synthesized biocomposite that uses materials from secondary resources (orange-peel) can be successfully used in the selective removal of phenol from compounds of interest existing in agro-food wastewaters.

Declaration of Competing Interest

The authors declare no conflict of interest.

Acknowledgements

Appendix A. Supplementary data

Supplementary data to this article can be found online at https://doi.org/10.1016/j.colcom.2021.100402.

References

[1] G. Ait Baddi, J. Cegarra, G. Merlina, J.C. Revel, M. Hafidi, Qualitative and quantitative evolution of polyphenolic compounds during composting of an olive-mill waste–wheat straw mixture, J. Hazard. Mater. 165 (2009) 1119–1123, https://doi.org/10.1016/j.jhazmat.2008.10.102.

[2] L. Bertin, F. Ferri, A. Scoma, L. Marchetti, F. Fava, Recovery of high added value natural polyphenols from actual olive mill wastewater through solid-phase extraction, Spec. Sect. Symp. Post-Combust. Carbon Dioxide Capture 171 (2011) 1287–1293, https://doi.org/10.1016/j.cej.2011.05.056.

[3] M. Stoller, Effective fouling inhibition by critical flux based optimization methods on a NF membrane module for olive mill wastewater treatment, Chem. Eng. J. 168 (2011) 1140–1148, https://doi.org/10.1016/j.cej.2011.01.098.

[4] A. Cicci, M. Stoller, M. Bravi, Microalgal biomass production by using ultra- and nanofiltration membrane fractions of olive mill wastewater, Water Res. 47 (2013) 4710–4718, https://doi.org/10.1016/j.watres.2013.05.030.

[5] G. Busca, S. Berardinelli, C. Resini, L. Arrighi, Technologies for the removal of phenol from fluid streams: a short review of recent developments, J. Hazard. Mater. 160 (2008) 265–288, https://doi.org/10.1016/j.jhazmat.2008.03.045.

[6] A. Bendini, et al., Phenolic molecules in virgin olive oils: a survey of their sensory properties, health effects, antioxidant activity and analytical methods, Molecules 12 (2007) 1679–1719, https://doi.org/10.3390/12081679.

[7] J.M. Ochando-Pulido, M. Stoller, M. Bravi, A. Martinez-Ferez, A. Chianese, Batch membrane treatment of olive vegetation wastewater from two-phase olive oil production process by threshold flux based methods, Sep. Purif. Technol. 101 (2012) 34–41, https://doi.org/10.1016/j.seppur.2012.09.015.

[8] M. Stoller, M. Bravi, A. Chianese, Threshold flux measurements of a nanofiltration membrane module by critical flux data conversion, Spec. Issue Nanofiltration Membr. Fundam. Appl. 315 (2013) 142–148, https://doi.org/10.1016/j.desal.2012.11.013.

[9] A. Bhatnagar, M. Sillanpää, A. Witek-Krowiak, Agricultural waste peels as versatile biomass for water purification – A review, Chem. Eng. J. 270 (2015) 244–271, https://doi.org/10.1016/j.cej.2015.01.135.

[10] M. Ververi, A.M. Goula, Pomegranate peel and orange juice by-product as new biosorbents of phenolic compounds from olive mill wastewaters, Chem. Eng. Process. Intensif. 138 (2019) 86–96, https://doi.org/10.1016/j.cep.2019.03.010.

[11] L.M. Camacho, A. Torres, D. Saha, S. Deng, Adsorption equilibrium and kinetics of fluoride on sol–gel-derived activated alumina adsorbents, J. Colloid Interface Sci. 349 (2010) 307–313, https://doi.org/10.1016/j.jcis.2010.05.066.

[12] J. Du, D.A. Sabatini, E.C. Butler, Synthesis, characterization, and evaluation of simple aluminum-based adsorbents for fluoride removal from drinking water, Chemosphere 101 (2014) 21–27, https://doi.org/10.1016/j.chemosphere.2013.12.027.

[13] S. Zahra, S. Reyhane, F. Reza, Fixed-bed adsorption dynamic of Pb(II) adsorption from aqueous solution using nanostructured γ-alumina, J. Nanostruct. Chem. (2013) 1–8. link.springer.com. https://doi.org/10.1186/2193-8865-3-48.

[14] F. Gottschalk, T. Sun, B. Nowack, Environmental concentrations of engineered nanomaterials: review of modeling and analytical studies, Environ. Pollut. 181 (2013) 287–300, https://doi.org/10.1016/j.envpol.2013.06.003.

[15] L. Joseph, J.R.V. Flora, Y.-G. Park, M. Badawy, H. Saleh, Y. Yoon, Removal of natural organic matter from potential drinking water sources by combined coagulation and adsorption using carbon nanomaterials, Sep. Purif. Technol. 95 (2012) 64–72, https://doi.org/10.1016/j.seppur.2012.04.033.

[16] J.R. Njimou, A. Măicăneanu, C. Indolean, C.P. Nanseu-Njiki, E. Ngameni, Removal of Cd (II) from synthetic wastewater by alginate - Ayous sawdust (*Triplochiton scleroxylon*) composite material, Environ. Technol. 37 (2016) 1369–1381, https://doi.org/10.1080/09593330.2015.1116609.

[17] A. Yangui, J.R. Njimou, A. Cicci, M. Bravi, M. Abderrabba, A. Chianese, Competitive adsorption, selectivity and separation of valuable hydroxytyrosol and toxic phenol from olive mill wastewater, J. Environ. Chem. Eng. 5 (2017) 3581–3589, https://doi.org/10.1016/j.jece.2017.06.037.

[18] E. Tchomgui-Kamga, V. Alonzo, C.P. Nanseu-Njiki, N. Audebrand, E. Ngameni, A. Darchen, Preparation and characterization of charcoals that contain dispersed aluminum oxide as adsorbents for removal of fluoride from drinking water, Carbon 48 (2010) 333–343, https://doi.org/10.1016/j.carbon.2009.09.034.

[19] E. Tchomgui-Kamga, E. Ngameni, A. Darchen, Evaluation of removal efficiency of fluoride from aqueous solution using new charcoals that contain calcium compounds, J. Colloid Interface Sci. 346 (2010) 494–499, https://doi.org/10.1016/j.jcis.2010.01.088.

[20] N. Horny, Y. Kanake, M. Chirtoc, L. Tighzert, Optimization of thermal and mechanical properties of biopolymer-based nanocomposites, Polym. Degrad. Stab. 127 (2016) 105–112, https://doi.org/10.1016/j.polymdegradstab.2016.01.006.

[21] M. Chirtoc, N. Horny, I. Tavman, A. Turgut, I. Kökey, N. Omastová, Preparation and photothermal characterization of nanocomposites based on high-density polyethylene filled with expanded and unexpanded graphite: particle size and shape effects, Therm. Mater. Nanosci. Nanotechnol. 62 (2012) 50–55, https://doi.org/10.1016/j.ijthermalsci.2012.02.015.

[22] A.E. Ofomaja, Y.-S. Ho, Effect of temperatures and pH on methyl violet biosorption by Mansonia wood sawdust, Bioresour. Technol. 99 (2008) 5411–5417, https://doi.org/10.1016/j.biortech.2007.11.018.

[23] K.C. Nebaghe, Y. El Boundati, K. Ziat, A. Naji, L. Rghioui, M. Saidi, Comparison of linear and non-linear method for determination of optimum equilibrium isotherm for adsorption of copper(II) onto treated Martil sand, Fluid Phase Equilib. 430 (2016) 188–194, https://doi.org/10.1016/j.fluid.2016.10.003.

[24] M. Ge, X. Wang, M. Du, G. Liang, G. Hu, S.M. Jahangir Alam, Adsorption analyses of phenol from aqueous solutions using magadiite modified with organo-functional groups: kinetic and equilibrium studies, Materials 12 (2019) 96, https://doi.org/10.3390/ma12010096.

[25] J.R. Njimou, Martin Pengou, H.K. Tchakouté, Ulrich Fannang, C. Tizaoui, M.T. Sieugaing, P.N. Lemougna, C.P. Nanseu-Njiki, E. Ngameni, Removal of lead ions from aqueous solution by phosphate-based geopolymer cement composite, J. Chem. Technol. Biotechnol. xx (2021) 1–12.

[26] Y.N. Mata, M.L. Blázquez, A. Ballester, F. González, J.A. Muñoz, Biosorption of cadmium, lead and copper with calcium alginate xerogels and immobilized Fucus vesiculosus, J. Hazard. Mater. 163 (2009) 555–562, https://doi.org/10.1016/j.jhazmat.2008.07.015.

[27] M. Bhaumik, K. Setshedi, A. Maity, M.S. Onyango, Chromium(VI) removal from water using fixed bed column of polypyrrole/Fe$_3$O$_4$ nanocomposite, Sep. Purif. Technol. 110 (2013) 11–19, https://doi.org/10.1016/j.seppur.2013.02.037.

[28] J.E. Mbosso, A. Măicăneanu, C. Indolean, J.R. Njimou, C. Majdik, Cd^{2+} removal from aqueous solutions using an organo-inorganic immobilized adsorbent, Rev. Roum. Chim. 57 (2012) 321–325. http://web.icf.ro/rrch.

[29] T.K. Sherwood, R.L. Pigford, C.R. Wilke, Mass Transfer, Mc Graw-Hill, Inc. New York, 1975.

[30] M.C. Annesini, F. Gironi, B. Monticelli, Removal of oxygenated pollutants from wastewater by polymeric resins: data on adsorption equilibrium and kinetics in fixed beds, Water Res. 34 (2000) 2989–2996, https://doi.org/10.1016/S0043-1354(00)00047-6.

[31] U.F. Alkaram, A.A. Mukhlis, A.H. Al-Dujaili, The removal of phenol from aqueous solutions by adsorption using surfactant-modified bentonite and kaolinite, J. Hazard. Mater. 169 (2009) 324–332, https://doi.org/10.1016/j.jhazmat.2009.03.153.

[32] R. Liu, R.L. Frost, W.N. Martens, Y. Yuan, Synthesis, characterization of mono, di and tri alkyl surfactant intercalated Wyoming montmorillonite for the removal of phenol from aqueous systems, J. Colloid Interface Sci. 327 (2008) 287–294, https://doi.org/10.1016/j.jcis.2008.08.049.

[33] B. Chang, W. Shi, D. Guan, Y. Wang, B. Zhou, X. Dong, Hollow porous carbon sphere prepared by a facile activation method and its rapid phenol removal, Mater. Lett. 126 (2014) 13–16, https://doi.org/10.1016/j.matlet.2014.03.177.

[34] B. Taraba, P. Bulavová, Adsorption enthalpy of lead(II) and phenol on coals and activated carbon in the view of thermodynamic analysis and calorimetric measurements, J. Chem. Thermodyn. 116 (2018) 97–106, https://doi.org/10.1016/j.jct.2017.08.026.

[35] W.A. Cabrera-Lafaurie, F.R. Román, A.J. Hernández-Maldonado, Single and multi-component adsorption of salicylic acid, clofibric acid, carbamazepine and caffeine from water onto transition metal modified and partially calcined inorganic-organic pillared clay fixed beds, J. Hazard. Mater. 282 (2014) 174–182, https://doi.org/10.1016/j.jhazmat.2014.03.0092014.

[36] A.H. Sulaymon, S.A. Yousif, M.M. Al-Faize, Competitive biosorption of lead mercury chromium and arsenic ions onto activated sludge in fixed bed adsorber, J. Taiwan Inst. Chem. Eng. 45 (2014) 325–337, https://doi.org/10.1016/j.jtice.2013.06.034.

[37] P. Bingcai, et al., Sorption enhancement of aromatic sulfonates onto an aminated hyper-cross-linked polymer, Environ. Sci. Technol. (2005) 3308–3313, https://doi.org/10.1021/es048548j.

[38] P.-J. Lu, C.-S. Chang, J.-M. Chern, Binary adsorption breakthrough curves in fixed bed: experiment and prediction, J. Taiwan Inst. Chem. Eng. 45 (2014) 1608–1617, https://doi.org/10.1016/j.jtice.2013.10.018.

[39] L. Lv, K. Wang, X.S. Zhao, Effect of operating conditions on the removal of Pb^{2+} by microporous titanosilicate ETS-10 in a fixed-bed column, J. Colloid Interface Sci. 305 (2007) 218–225, https://doi.org/10.1016/j.jcis.2006.09.053.

[40] A. Wolborska, P. Pustelnik, A simplified method for determination of the breakthrough time of an adsorbent layer, Water Res. (1996) 2643–2650, https://doi.org/10.1016/S0043-1354(96)00166-2.

[41] C. Valderrama, J.L. Cortina, A. Farran, X. Gamisans, F.X. de las Heras, Kinetic study of acid red "dye" removal by activated carbon and hyper-cross-linked polymeric sorbents Macronet Hypersol MN200 and MN300, React. Funct. Polym. 68 (2008) 718–731, https://doi.org/10.1016/j.reactfunctpolym.2007.11.013.

[42] C. Valderrama, J.L. Cortina, A. Farran, X. Gamisans, F.X. de las Heras, Evaluation of hyper-cross-linked polymeric sorbents (Macronet MN200 and MN300) on dye (Acid red 14) removal process, React. Funct. Polym. 68 (2008) 679–691, https://doi.org/10.1016/j.reactfunctpolym.2007.11.005.

[43] C. Valderrama-Bravo, et al., Mechanism of calcium uptake in corn kernels during the traditional nixtamalization process: diffusion, accumulation and percolation, J. Food Eng. 98 (2010) 126–132, https://doi.org/10.1016/j.jfoodeng.2009.12.018.

[44] T.J. Buran, A.K. Sandhu, Z. Li, C.R. Rock, W.W. Yang, L. Gu, Adsorption/desorption characteristics and separation of anthocyanins and polyphenols from blueberries using macroporous adsorbent resins, J. Food Eng. 128 (2014) 167–173, https://doi.org/10.1016/j.jfoodeng.2013.12.029.

[45] J. Huang, X. Wu, H. Zha, B. Yuan, S. Deng, A hypercrosslinked poly(styrene-co-divinylbenzene) PS resin as a specific polymeric adsorbent for adsorption of 2-naphthol from aqueous solutions, Chem. Eng. J. 218 (2013) 267–275, https://doi.org/10.1016/j.cej.2012.12.032.

[46] C. Valderrama, J.I. Barios, M. Caetano, A. Farran, J.L. Cortina, Kinetic evaluation of phenol/aniline mixtures adsorption from aqueous solutions onto activated carbon and hypercrosslinked polymeric resin (MN200), React. Funct. Polym. 70 (2010) 142–150, https://doi.org/10.1016/j.reactfunctpolym.2009.11.003.

[47] J.R. Njimou, F.N. Kouatchie, E. Njungab, A. Talla, Nkeng G. Elambo, Treatment of Agro-Food Wastewaters and Valuable Compounds Recovery by Column Sorption Runs, in Sorption in 2020s, Éd. Rijeka: IntechOpen, 2020, https://doi.org/10.5772/intechopen.90087. Ch. 5.

[48] M. Stoller, M. Bravi, Critical flux analyses on differently pretreated olive vegetation waste water streams: some case studies, Desalination 250 (2010) 578–582, https://doi.org/10.1016/j.desal.2009.09.027.

[49] M.L. Soto, A. Moure, H. Domínguez, J.C. Parajó, Recovery, concentration and purification of phenolic compounds by adsorption: a review, J. Food Eng. 105 (2011) 1–27, https://doi.org/10.1016/j.jfoodeng.2011.02.010.

[50] M. Jain, V.K. Garg, K. Kadirvelu, Cadmium (II) sorption and desorption in a fixed bed column using sunflower waste carbon calcium–alginate beads, Bioresour. Technol. 129 (2013) 242–248, https://doi.org/10.1016/j.biortech.2012.11.036.